ISSN 0167-6636

ELSEVIER

MECHANICS OF MATERIALS

AN INTERNATIONAL JOURNAL

Forum for original scientific research on the flow, fracture, and general constitutive behavior of advanced technological and natural materials

Volume 71, April 2014

Mechanics of Materials 71 (2014) 101–113

Contents lists available at ScienceDirect

Mechanics of Materials

journal homepage: www.elsevier.com/locate/mechmat

An experimental study on the mechanical behaviour of two polyurethane resins used for geotechnical applications

R. Valentino [a,⇑], E. Romeo [a], D. Stevanoni [b]

[a] Department of Civil, Environmental, Territory Engineering and Architecture, University of Parma, Viale G.P. Usberti 181/A, 43100 Parma, Italy
[b] Novatek s.r.l., Via dell'Artigianato 11, 37021 Bosco Chiesanuova (VR), Italy

article info

Article history:
Received 25 July 2013
Received in revised form 16 December 2013
Available online 2 February 2014

Keywords:
Polyurethane resins
Geotechnical works
Foundation reinforcement
Mechanical behaviour

abstract

The objective of this paper is to experimentally investigate the mechanical behaviour of different polyurethane expanding resins, which are widely used for ground improvement and foundation remediation. This study is the first step towards the primary objective, which is to define a design procedure for this type of intervention. This study encompasses two goals: (1) develop a relationship between the density of the resin and the confinement pressure in expansion conditions, and (2) measure the mechanical parameters from simple compression tests on resin specimens. Experimental tests were performed on two different types of resin, and the results reveal that the higher the confinement stress is during the expansion phase, the greater the hardened resin density. Moreover, the resin density and confinement stress are linked by a well-defined law. The laboratory tests show how the stress–strain behaviour is strongly non-linear and that both the elastic and strength parameters greatly depend on the boundary conditions during the expansion phase.

1. Introduction

In the field of geotechnical and structural engineering, the settlement of shallow foundations, which subsequently deforms existing buildings, is a widespread problem that often requires rapid solutions with the lowest level of disturbance. The necessity of reinforcing railway or motorway embankments and airstrips to improve substructure performance is also a frequent challenge for civil engineers. At present, different systems based on innovative technologies can enhance the load capacity of a shallow foundation or limit the compressibility of the subsoil, both in the short and long term. A recently proposed method is based on using polyurethane expanding resins, which are injected into the subsoil beneath the base of a shallow foundation (Buzzi et al., 2008, 2010). In most cases, this type of remediation technique is performed without a preliminary design procedure and only on the basis of experience, i.e., this technique is merely an empirical approach. In fact, there is only a small amount of scientific knowledge available regarding the combined behaviour of soil and polyurethane resins. The experimental research described in this paper contributes to the study of polyurethane resins, which are specifically used for geotechnical works, with the awareness that a deeper investigation is required to define a standard design procedure for this type of ground improvement technique.

Polyurethane resins belong to the category of foam materials, whose common attributes are high porosity, a light weight, high crushability, and a good deformation energy absorption capacity. These resins are essentially made of interconnected networks of solid struts and cell walls interspersed by voids with entrapped gas and are generally classified as either ''open'' or ''closed'' cell foams (Tu et al., 2001; Buzzi et al., 2008).

⇑ Corresponding author. Tel.: +39 0521 906112; fax: +39 0521 905924.
E-mail addresses: roberto.valentino@unipr.it (R. Valentino), elena.romeo@unipr.it (E. Romeo), davide.stevanoni@novatek.it (D. Stevanoni).

http://dx.doi.org/10.1016/j.mechmat.2014.01.007
0167-6636/

It must be mentioned that there have been studies on the mechanical properties of polyurethane resins that have been extensively documented over the last two decades (Hilyard and Cunningham, 1994; Gibson and Ashby, 1997). In most cases, the emphasis is on the compressive behaviour and the energy absorption characteristics of foams undergoing large dynamic deformations. In fact, due to their high energy absorption capabilities, polyurethane foams have been widely used in packaging and cushioning to protect sensitive objects.

Rigid polyurethane foams are also used as thermal insulation or structural materials for various applications.

Thanks to the wide range of industrial applications, the mechanical behaviour of polyurethane resins has been investigated by many engineers and researchers. Gibson and Ashby (1997) provided an extensive survey on different types of cellular materials, which ranged from packaging to lightweight structures, and discussed the complexity of foam deformation and offered many insights into the relationship between the microstructure geometry and material properties. The authors also addressed two possible failure modes under compression and subsequently developed models correlating the bulk properties and foam microstructures for each failure mode.

Because the ability to predict failure of cellular materials depends on the knowledge of the microstructural mechanisms, which contribute to their macroscopic behaviour, Ford and Gibson (1998) also developed microstructural models to examine the mechanisms responsible for differences in tensile and compressive strength observed in cellular materials.

In the framework of foam materials, Daniel and Cho (2011) described a quasi-static, dynamic characterisation of an anisotropic PVC foam used for composite sandwich structures. The authors conducted uniaxial stress and uniaxial strain experiments and proposed a simplified model to predict the Young's modulus.

Regarding large dynamic deformations, Zhang et al. (1998) presented selected experimental results on low-density polyurethane foams and developed a rate-dependent hydrodynamic constitutive equation for rigid polymeric foams. Tu et al. (2001) experimentally examined the mechanical response of rigid polyurethane foam to compression in the rise and transverse directions. In fact, the authors attributed the difference in deformation to anisotropy in the internal cellular structure that arises from the fabrication process. To describe deformation localisation in the rise direction of the foam, the authors proposed a simple theoretical analysis that used the concept of deformation bands.

Saha et al. (2005) discussed the compression behaviour of two classes of polymer foams with different densities (320 kg/m ^{3} and 240 kg/m ^{3}, respectively) for an extremely wide range of strain rates, with an emphasis on the peak stress and energy absorption. The authors stated that both foams showed a negligible effect of the strain rate on the peak stress and energy absorption.

To support and enhance industrial processes, several researchers have studied the production of polyurethane foam with a complex geometry. As an example, a theoretical model, which includes the chemical reactions, foaming and mould filling, was developed by Seo and Youn (2005) to analyse the foam reaction injection moulding. The authors derived an energy balance equation by considering a polyurethane reaction, a water–isocyanate reaction, and the evaporation of physical blowing agents and proposed a density and viscosity model for bubble suspension. Based on the theoretical model, the authors performed a three-dimensional numerical simulation for mould filling of a polyurethane foam to predict the flow field, flow front advancement, and density distribution during mould filling of a refrigerator cavity.

In this paper, two types of polyurethane resins that are commonly used for geotechnical applications are examined. The first objective is to determine, for each analysed resin type, the relationship between the confinement pressure and density of the resin in the solid state; the second objective is to study the mechanical behaviour of different types of resins under compression loading. Quasi-static compression tests were performed using a servo-hydraulic material testing system (MTS). All resin specimens were tested in the rise direction, and the stress–strain responses were established to determine the peak stress, Young's modulus and fracture energy.

2. Materials and testing

2.1. Polyurethane resins

The tested expanding polyurethane resin that was used, which is abbreviated HDR ^{Ò} (high-density resin, EU trademark No. 3790862), is a two-component resin created through a mixture of polyol and diphenylmethane diisocyanate in specified quantities. When the two components of the mixture (originally in liquid state) combine with each other, they induce a high-speed chemical reaction that quickly determines the expansion of the injected product that can increase its volume from 1.2 to 40 times its original volume.

As a result of the water dosage in the mixture, it is possible to determine the final properties of the resin. Indeed, water acts as a blowing agent in the chemical reaction, speeding up the expansion and the solidification process. Different confinement conditions determine different expansion pressures and the ultimate density of the resin. The characteristics of the resin analysed in this research and used for the field injections are reported in Table 1. The primary factors that affect the reaction are the following: the mixing ratio of the two chemical components, temperature, and surrounding pressure. The technique adopted in the field applications allows the first two variables to be fixed (i.e., mixing ratio of the two chemical

Table 1
Properties of the expanding polyurethane resin.

Property	Value
Mass per unit volume in free expansion (kg/m ^{3})	30–220
Temperature at mixing (°C)	30–50
Mixing pressure (bar)	40–60
Injecting pressure (bar)	5–10

components and temperature); however, the surrounding pressure depends on both the depth of the injection point with respect to the ground level and the existing external loads. During the chemical reaction, the volume of the material considerably increases due to the reaction between excess diisocyanate and water, which subsequently produces carbon dioxide. The presence of carbon dioxide provides the final resin with the typical closed-cell structure (Valentino et al., 2013; Buzzi et al., 2008).

Two types of polyurethane resin, referred to as HDR-A and HDR-B, were examined. Their specific characteristics will be described in the section concerning the test program. The HDR-A type is expected to be characterised by a relatively high expansion power compared with that of the HDR-B type. Fig. 1 shows three resin HDR-A samples that were obtained at different confinement pressures, which will be explained in the following section.

2.2. Experimental set-up

The first objective of the present study is to determine the relationship between confinement pressure (p_{HDR}) and the density of each type of analysed resin at the solid state (q_{HDR}) while maintaining both a constant temperature and mixing ratio of the components. The confinement pressure is defined as the pressure incurred by the resin during the injection and expansion phases. In geotechnical applications, it is expected that this pressure will be proportional to both the depth of the injection point and overloads at the foundation level. The second objective is to study the mechanical behaviour of the types of resin at different confinement conditions using uniaxial compression tests.

2.2.1. Apparatus for preparing the resin specimens

Pressures commonly encountered in field applications were artificially reproduced in the laboratory. For this purpose, an ad hoc instrument (HDR pressure device) was set up (Fig. 2). The HDR pressure device allows resin samples to be created at different confinement conditions during injection and expansion at a well-defined, user-imposed pressure level. Moreover, the device allows the same boundary conditions to be replicated to verify the experimental repeatability. It must be underlined that the HDR pressure device does not reproduce actual site conditions

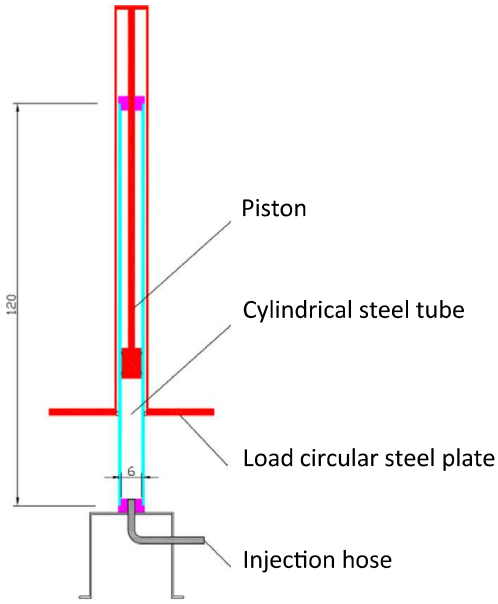

Fig. 2. Sketch of the HDR pressure device to produce resin samples at different confinement conditions (dimensions are in cm).

of ''free injection'' because radial expansion is blocked and only vertical free expansion is allowed. Nevertheless, the HDR pressure device allows resin samples to be prepared under different surrounding conditions that can then be characterised by different properties.

The HDR pressure device consists of a cylindrical steel tube 1.2 m in length and 0.07 m in diameter. The edge of the injection hose is seated at the bottom tip of the tube (Fig. 2). The resin at the initial liquid state is injected in the inner hollow of the tube through the bottom hose. The inner hollow is closed on the top by a piston, which can translate along the vertical axis of the cylinder.

The volume of the void space initially available for the resin to expand is equal to 5.65 Â 10 ^{Å4} m^3. The presence of this initial quantity of air is required for the chemical reaction. A small quantity of lubricating oil minimises the friction when the piston is lifted. The piston head is rigidly connected with a second external hollow tube, which has a greater diameter and is coaxial with the first one. The external hollow tube is able to translate vertically together with the inner piston. At the base of the external cylinder, a

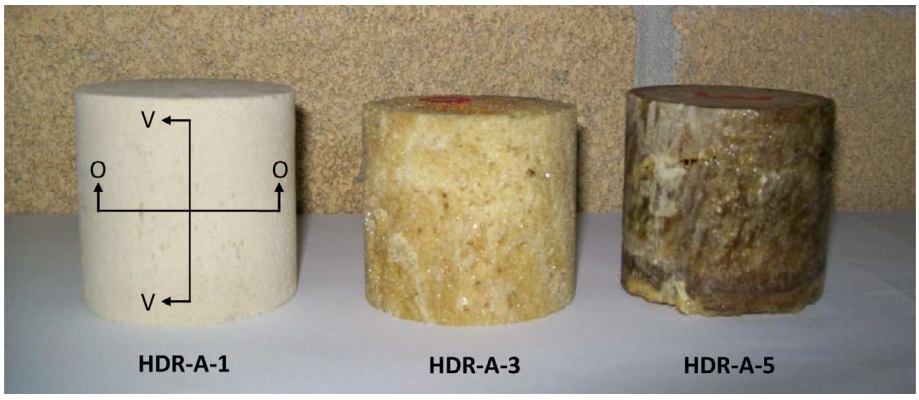

Fig. 1. Samples of resin HDR-A obtained at different confinement pressures (Table 2).

circular steel plate is rigidly connected. To obtain the desired pressure on the piston, different weights can be positioned on the plate (Fig. 2).

The HDR pressure device has been used to make resin samples that are characterised by different confinement pressures (p_{HDR}). In particular, by applying a fixed load at the top of the piston, it was possible to evaluate the reaction stress applied by the resin on the lifting piston. The calculated applied stress also accounted for the weight of the apparatus itself. The friction stress between the inner piston and the external cylinder was also evaluated.

A second series of resin samples was prepared by injecting the resin in an open box to obtain expansion at atmospheric pressure (unconfined expansion). A total of 54 specimens of the two types of resins were obtained using both the confined and unconfined expansion method (Table 2).

2.2.2. Apparatus for UCS tests

The unconfined compression strength test (UCS) was performed using an MTS closed-loop servo-hydraulic loading system using a 250 kN load cell. Two HBM-Y series strain gauges, which were arranged in a quarter Wheatstone bridge with a length of 8 mm, were mounted on the central section of the specimen to measure the radial deformations during testing. The experimental setup is shown in Fig. 3.

The strain gauge signals were acquired by a National Instrument SCXI Chassis, which can scan input channels at rates up to 333 kS/s. A commercial software developed in a LabView environment was used to calculate the strain gauge parameters and acquire the output signals. Failure is defined as the point on the stress–strain curve where the load reaches its maximum during the elastic phase, i.e., the yielding point. The load at failure (P_u) was recorded, and the uniaxial compressive stress at failure (σ_u) was determined by dividing P_u by the cross-sectional area of the specimen.

From the test results, it was possible to evaluate the behaviour of each resin in terms of its stress–axial strain response, stress–radial strain behaviour and dissipated energy to failure according to the confinement pressure.

2.3. Testing program and conditions

The two different types of resin (HDR-A and HDR-B) were tested in a laboratory by performing an UCS test. For this purpose, 44 of the 54 resin specimens were tested.

Table 2
Details of the tested specimens and conditions.

Expansion	Resin type	Structure	N. specimens	p_{HDR}* (kPa)
Unconfined	HDR-A	Cellular	13	0
	HDR-B	Cellular	7	0
Confined	HDR-A-1	Cellular	5	100
	HDR-A-3	Cellular	3	300
	HDR-A-5	Cellular	5	465
	HDR-A-10	Cellular	3	935
	HDR-B-1	Rigid	10	100
	HDR-B-3	Rigid	8	300

* Relative pressure with respect to the atmospheric pressure.

Fig. 3. UCS experimental set-up.

Each resin specimen had a well-defined cylindrical shape. The resin density, which ranged between 34 kg/m^3 and 1056 kg/m^3, was calculated for each specimen after being weighed (Table 3). The primary characteristics of the tested specimens are reported in Tables 2 and 3. All specimens were divided into two categories on the basis of both their density and microstructure. In particular, the structure was defined as ''cellular'' for a specimen whose density was less than 700 kg/m^3 and ''rigid'' for a density greater than this value. The specimen classification was also performed on the basis of the microstructure analysis by considering the presence of a closed-cell (cellular) structure or a dense (rigid) structure, which will be subsequently explained.

It was expected that the two resins would exhibit different strength levels. In particular, the HDR-A type was expected to be characterised by a lower strength level than that of the HDR-B type at the same confinement pressure.

Because the structure of the obtained samples can be divided in two main types (cellular and rigid), two different standard test methods were performed to determine the compressive properties: the ASTM 1621-04a standard was used for the cellular resin, and the ASTM D 695-08 standard was used for the rigid resin. Following the standards, two different dimensions were adopted for the mechanical tests on the cylindrical specimens. In particular, the cellular resin specimens had a diameter of 60 mm and a height 60 mm (in agreement with ASTM 1621-04a); the rigid resin specimens had a diameter of 30 mm and a height of 60 mm (in agreement with ASTM D 695-08). The load transmission was controlled by a displacement control system, where the top plate of the MTS dropped at a speed of 5.4 mm/min (ASTM 1621-04a) or at a speed of 1.3 mm/min (ASTM D 695-08). The number of replicates of the tested resins varied according to the available number of specimens.

3. Results

3.1. Expansion process

In the first stage of this study, two reference states of the resin were considered for the analyses. First, the resin

Table 3
Mechanical performance of specimens in the HDR pressure device.

Resin type	N. specimens	p_{HDR}* (kPa)	ρ_{HDR} (mean) (kg/m^3)	L (kJ)	L_{mean} (kJ)	St. dev. (L)	St. dev. (L_{mean})
HDR-A	13	0	34	2.942	2.942	0.320	0.320
HDR-B	7	0	215	0.385	0.385	0.016	0.016
HDR-A-1	5	100	243	0.658	0.693	0.064	0.088
HDR-A-3	3	300	368	0.763		0.142	
HDR-A-5	5	465	483	0.690		0.097	
HDR-A-10	3	935	656	0.687		0.029	
HDR-B-1	10	100	995	0.029	0.031	0.007	0.0067
HDR-B-3	8	300	1056	0.034		0.006	

* Relative pressure with respect to the atmospheric pressure.

Table 4
Material parameters.

Resin type	Expansion	x_w (%)	x_{CO_2} (%)	M_{no}* (g/mol)	M_{CO_2}* (g/mol)	M_{H_2O} (g/mol)	ρ_w (kg/m^3)	ρ_L(kg/m^3)T *(K)	R_g(J/molÁK)
HDR-A	Confined	0.1	12	615	44	18.015	1000	1159.4 398.15	8.314
HDR-B	Confined	0.1	0.7	615	44	18.015	1000	1159.4 398.15	8.314

* Baser and Khakhar (1994a) (T = 125 °C at the end of blown foam dynamics).

was at a liquid state before the chemical reaction when the two components were mixed. After the expansion reaction, the resin was at a solid state. For each state, the following physical quantities can be determined: the mass of the injected mixture (m_L) and the mass of the produced resin (m_S); the volume occupied by the resin before (V_L) and after (V_S) the reaction; and the density of the liquid mixture (ρ_L) and of the solid resin (ρ_S). On the basis of these quantities and by assuming as a first approximation that both the chemical and thermal energy are negligible, it is possible to calculate the mechanical energy used by the system during expansion. The mechanical work (L) done by a fixed quantity of the resin with a certain liquid mass (m_L), which expands at a confinement pressure (p), by passing from an initial liquid density (ρ_L) to a final solid density (ρ_S) and solid mass (m_S), can be calculated using the following equation:

$$L = \int_{V_{L;i}}^{V_{S;i}} p_i \, dV = p_i V_{S;i} - p_i V_{L;i} = p_i \frac{m_L}{\rho_{L;i}} - p_i \frac{m_S}{\rho_{S;i}} \quad (1)$$

where the subscript "i" represents every single reference state.

Because the density and the mixing ratio of the two chemical components are known, the density of the liquid mixture (ρ_L) can be easily calculated. The mass of the resin at a liquid state (m_L) can be reasonably considered equal to the mass of the resin at solid state (m_S), where the small mass of gas produced during the reaction is negligible. Then, by assuming $m_S = m_L = m$, the mechanical work is equal to the following:

$$L = p_i m \left(\frac{1}{\rho_{L;i}} - \frac{1}{\rho_{S;i}} \right) = p_i m \frac{\rho_{S;i} - \rho_{L;i}}{\rho_{L;i}\rho_{S;i}} \quad (2)$$

Under the hypothesis that for the same type of resin, the mechanical work is constant, it is possible to represent the locus of points at the same mechanical work obtained through Eq. (2). From Eq. (2), the density of the resin at solid state ($\rho_{s,i}$) can be obtained as follows:

$$\rho_{S;i} = \frac{p_i \cdot m \cdot \rho_{L;i}}{p_i \cdot m - L \cdot \rho_{L;i}} \quad (3)$$

where the density ρ_L and the mechanical work (L) for a representative unit mass of a resin are known.

Under these simplified hypotheses, the confinement pressure (p_i) and the final resin density (ρ_S) are linked to each other through the mechanical work (L). It has been assumed that the relationship can be represented on the (p; ρ) plane by a locus, which is given by the points at which the mechanical work is constant. This hypothesis will be validated by experimental results, which will be explained in the following section. By considering constant the mechanical work used during expansion at different confinement pressures and by considering two physical states labelled as state-1 and state-2, respectively, it is simple to demonstrate how the relationship is independent of mass:

$$\begin{cases} L_1 = p_1 m \frac{\rho_{S;1} - \rho_L}{\rho_L \cdot \rho_{S;1}} \\ L_2 = p_2 m \frac{\rho_{S;2} - \rho_L}{\rho_L \cdot \rho_{S;2}} \\ L_1 = L_2 \end{cases} \quad (4)$$

$$p_1 m \frac{\rho_{S;1} - \rho_L}{\rho_L \cdot \rho_{S;1}} = p_2 m \frac{\rho_{S;2} - \rho_L}{\rho_L \cdot \rho_{S;2}} \quad (5)$$

and then it follows:

$$\rho_{S;2} = \frac{p_2 \cdot \rho_{S;1} \cdot \rho_L}{p_1 \cdot \rho_L + p_2 \cdot \rho_{S;1} - p_1 \cdot \rho_{S;1}} \quad (6)$$

Eq. (6) explains the link between the points representing two physical states of the locus on the (p; ρ) plane.

The results of the experimental tests on all the 54 specimens will be used to validate the model. The resin specimens were obtained through expansion at two different conditions: confined conditions, given by the surrounding stress in the HDR pressure device, and the unconfined conditions at atmospheric pressure.

For each specimen, the density (ρ_{HDR}) was measured, and the mechanical work was calculated using Eq. (2). The calculated work is equal to the expansion work, which is given by the product between the confinement pressure, the horizontal section of the tube, and the piston rising. The results are summarised in Table 3. Due to the different number of replicates, the standard deviation of the calculated mechanical work, both for each type of specimen and for the mean work value, is also reported in Table 3. It can be observed that, in the confined conditions, the mechanical work is essentially the same for resin specimens of the same type at different confinement pressures. Fig. 4 reports the experimental measurements (dots) obtained for the two types of tested resins, HDR-A and HDR-B. Fig. 4 also shows the curves (solid lines) obtained from Eq. (3) by considering a constant value of the mechanical work (L) in confined conditions.

The experimental points that represent the resin specimens obtained in the unconfined conditions for the two types of resin are also plotted in Fig. 4. Indeed, for both resins, the unconfined conditions are represented by one experimental point, which does not fall on the model for the confined conditions. This gap suggests two remarks: firstly, it appears that the behaviour of the resins in the unconfined conditions is substantially different from that exhibited in confined conditions; secondly, the simplified assumptions do not allow the model to capture unconfined conditions, unless chemical and thermal work are included in addition to the mechanical work.

It can be observed that the curves have a horizontal asymptote that correspond to the liquid density of the mixture, ρ_L = 1159 kg/m^3. By comparing the curves at constant work with the experimental results, it can be observed that the simplified model appears appropriate for samples obtained under confinement pressures but is inappropriate for samples obtained under unconfined conditions.

The experimental data were also compared with the results of a well-established model, which represents the link between density and the confinement pressure, proposed by Baser and Khakhar (1994a,b). With the assumption of an ideal gas, this model takes into account not only the ambient pressure but also the temperature, mass fraction, and mole fraction of the blowing agent. The density of the free rising foam is given by

$$\rho_{S;i} = (1 + r_{w;0} + \frac{r_{CO_2} 1000 R_g T}{p M_{CO_2}} + \frac{r_w}{\rho_w} + \frac{1}{\rho_L})^{-1} \quad (7)$$

with

$$r_w = \frac{x_w}{(1 - x_w)} \frac{M_{H_2O}}{M_{no}} \quad (8)$$

and

$$r_{CO_2} = \frac{x_{CO_2}}{(1 - x_{CO_2})} \frac{M_{CO_2}}{M_{no}} \quad (9)$$

where p is the ambient pressure, r_w is the weight fraction of the water used as a blowing agent in the liquid phase, x_w is the mole fraction of the blowing agent (water), M_{H_2O} is the molecular weight of the blowing agent (water), r_{CO_2} is the weight fraction of the carbon dioxide, x_{CO_2} is the mole fraction of the carbon dioxide, M_{H_2O} is the molecular weight of the carbon dioxide, M_{no} is the initial number average molecular weight of the polymerising mixture, R_g is the gas law constant, T is the temperature, and ρ_w and ρ_L are the densities of water and resin at liquid state, respectively. In the HDR resin, the only blowing agent is water. Baser and Khakhar (1994a,b) used this model to describe the dynamics of polyurethane foam formation. The same model was used in this paper to describe the final state of the polyurethane foam formation process to determine a relationship between these states and different ambient pressures. By using the parameters reported in Table 4, Eq. (7) was plotted for the two types of resins (dashed lines in Fig. 4). In particular, the mole fraction of carbon dioxide (Table 5) is the only parameter that was estimated by considering that the quantity of carbon diox-

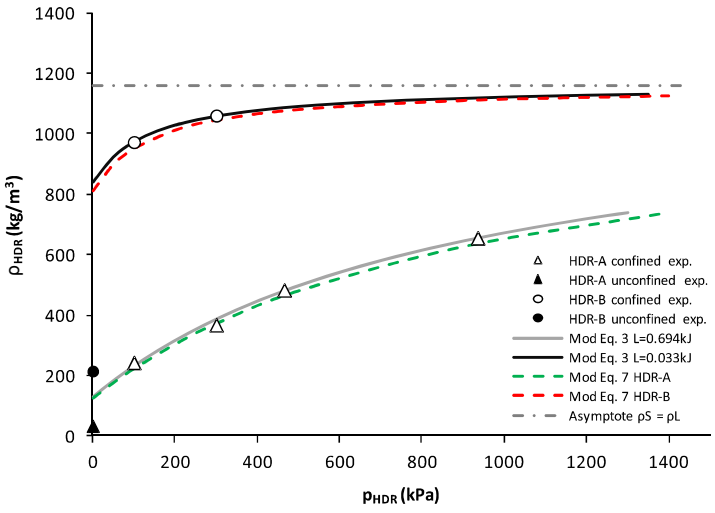

Fig. 4. Experimental measurements and relationship between ρ_{HDR} and p_{HDR} for the resins HDR-A and HDR-B. Solid lines are obtained from Eq. (3),by considering constant the value of the mechanical work (L); dashed lines are obtained from Eq. (7).

ide produced by the reaction for HDR-A is greater than that produced for HDR-B given their different expanding power. The mole fraction of the carbon dioxide for HDR-B is nearly 6% of that of HDR-A. On the contrary, the mole fraction of water was considered constant; however, it was negligible with respect to the carbon dioxide.

3.2. Microstructure

The microstructure of the two types of resin was analysed from images acquired through a scanning electron microscope (SEM). Figs. 5 and 6 show the microstructure of the two resins HDR-A and HDR-B, respectively, from specimens obtained under unconfined conditions. Both resins show the typical closed-cell structure, which has already been observed by Saha et al. (2005) and Buzzi et al. (2010). The primary difference is that the gas bubbles from the HDR-B specimens (Fig. 6) were smaller than those from the HDR-A specimens (Fig. 5). For specimens obtained under the unconfined conditions, the microstructure of both resins did not change with different directions (along sections O–O and V–V). In this case, the resin samples were characterised by a closed-cell structure, which appears homogeneous and isotropic. On the contrary, the microstructure of the resins exhibited extremely different characteristics for the specimens obtained in confined conditions. The resin samples obtained at low confinement pressures are again characterised by a closed-cell structure, which, in several cases, was anisotropic because the vertical direction is the only preferential direction of expansion. Moreover, the dimensions of the cells were different for different confinement pressures and different types of resin, which will be explained in the following section. Figs. 7 and 8 show specimens of the two types of resin (HDR-A-3 and HDR-B-3, respectively), both obtained at a confinement pressure of 300 kPa. In this case, the microstructure shows a certain anisotropy due to the method used to prepare the specimens in the HDR pressure device, where the expansion in the rise direction of the cylinder (V–V) is extremely different from that in the horizontal direction (O–O). In particular, Fig. 7a shows the microstructure of HDR-A-3 in the horizontal direction, which is not that different from that of Fig. 6a. Fig. 7b shows the microstructure of the same specimen of HDR-A-3 in the vertical direction: it is clearly evident how the gas bubble shape follows the rise direction (V–V). Fig. 8a and b show

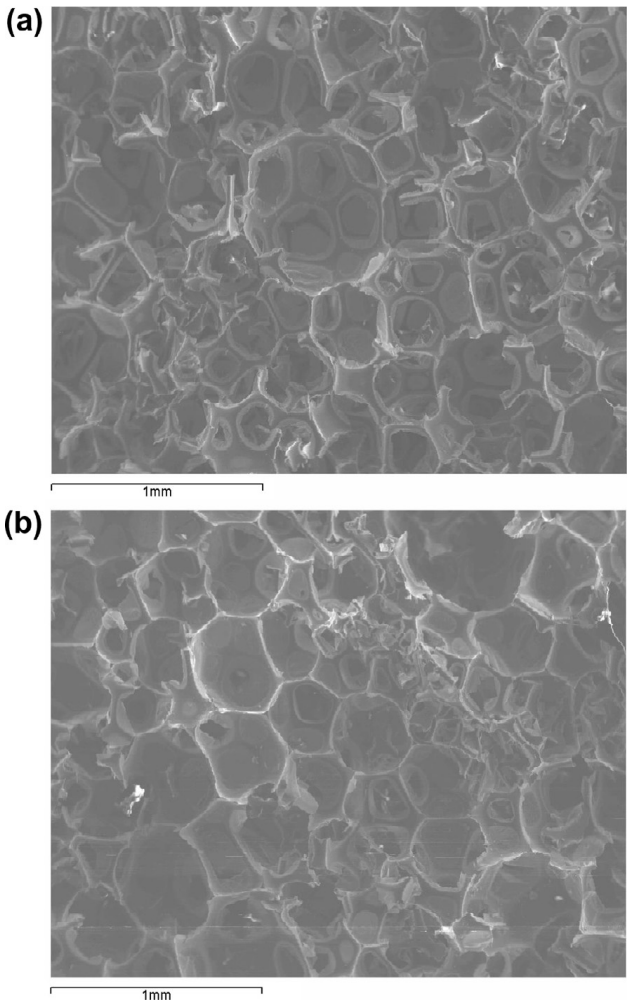

Fig. 5. SEM images of HDR-A resin samples obtained under unconfined conditions: (a) horizontal section (O–O in Fig. 1a); (b) vertical section (V–VinFig. 1a).

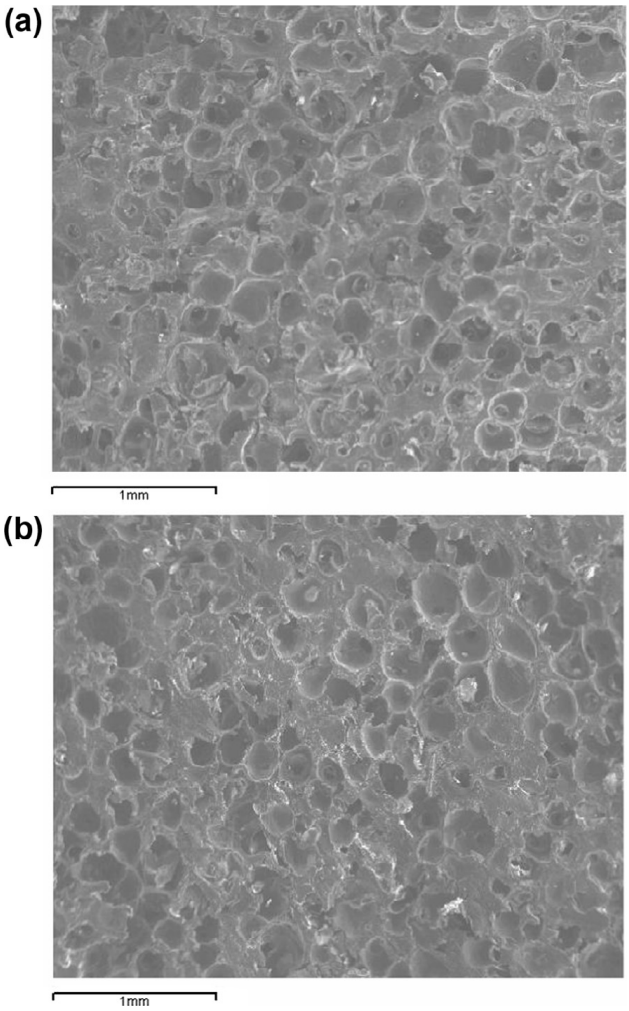

Fig. 6. SEM images of HDR-B resin samples obtained under unconfined conditions: (a) horizontal section (O–O in Fig. 1a); (b) vertical section (V–VinFig. 1a).

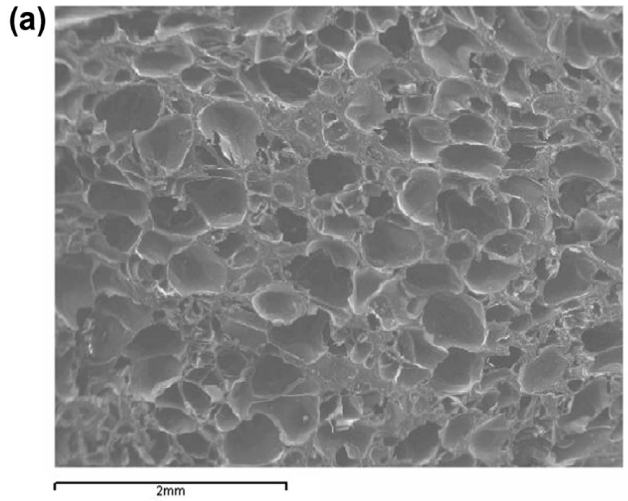

Fig. 7. SEM images of resin sample HDR-A-3: (a) section O–O (Fig. 1a); (b) section V–V (Fig. 1a).

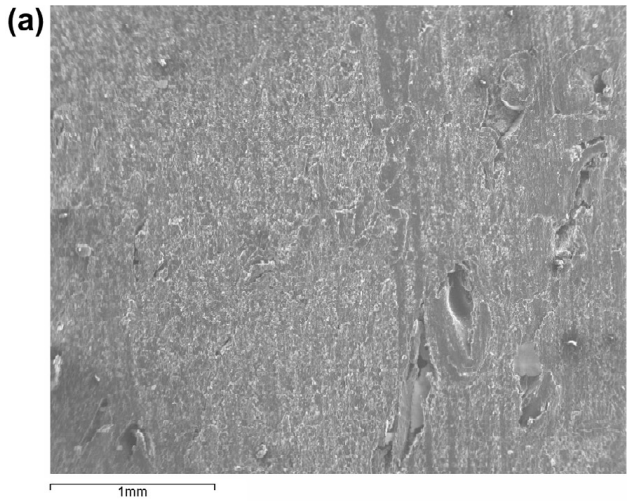

Fig. 8. SEM images of resin sample HDR-B-3: (a) section O–O (Fig. 1a); (b) section V–V (Fig. 1a).

the microstructure of HDR-B-3 in the horizontal and vertical directions, respectively. In this case, the microstructure is extremely different from that of HDR-A-3: gas bubbles are completely closed, and the resin structure appears dense and compact. The only sign of anisotropy is the long, narrow shape of the macro-voids in the vertical direction (Fig. 8b), which must be considered structure defects. At higher confinement pressures, the microstructure of HDR-A tends to exhibit the same characteristics of HDR-B, as shown by the SEM images in Fig. 9. Figs. Fig. Fig. 9a and b show the microstructure of HDR-A-10 in the horizontal and vertical directions, respectively. It can be observed that under this condition, the microstructure of HDR-A-10 is isotropic and extremely similar to that of HDR-B-3 (Fig. 8b).

3.3. Compression tests results

Among the 54 specimens tested in the first stage of the study, a series of 44 specimens were subjected to UCS tests. Figs. 10 and 11 show the stress–strain response of the HDR-A and HDR-B resins, respectively, on specimens obtained under confined expansion. The different curves are

Table 5
Mechanical performance of specimens from UCS tests.

Resin type	N. specimens	r_u (MPa)	E (MPa)	St. dev. (r_u)	St. dev. (E)
HDR-A	6	0.13	4.94	0.07	1.2
HDR-B	7	1.85	112.8	0.02	9.1
HDR-A-1	5	3.0	185	0.06	6.2
HDR-A-3	3	4.0	299	0.01	8.4
HDR-A-5	5	9.9	665	0.02	7.5
HDR-A-10	2	15.0	808	0.01	4.5
HDR-B-1	8	23.8	1423	1.2	25.3
HDR-B-3	7	32.5	1675	3.2	36.4

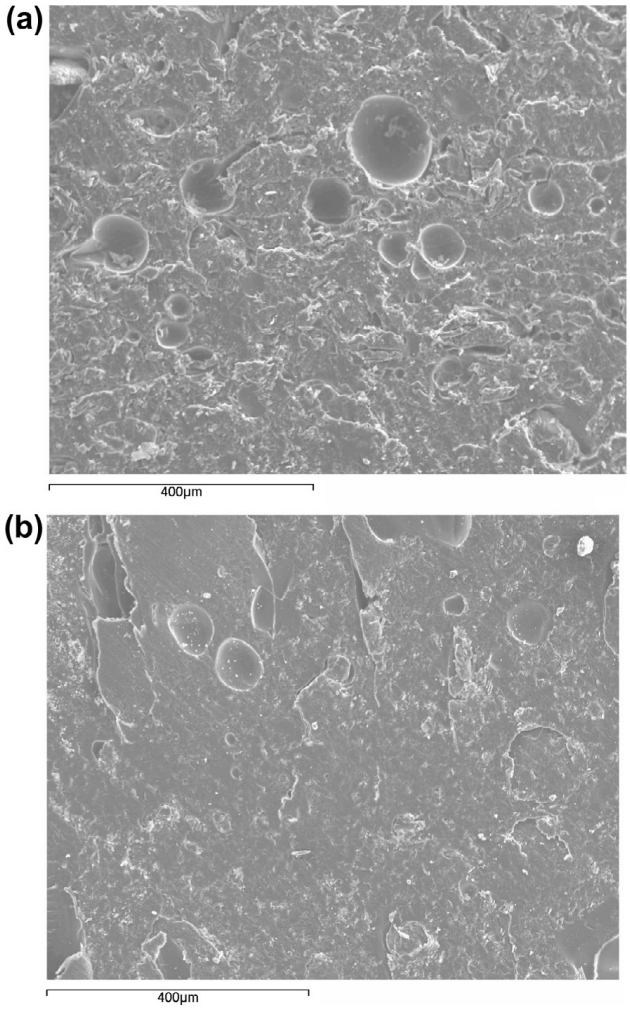

Fig. 9. SEM images of resin sample HDR-A-10: (a) section O–O (Fig. 1a); (b) section V–V (Fig. 1a).

associated with the different confinement pressures applied during specimen preparation. It can be observed that both failure stress and Young's modulus increase with the applied confinement pressure and thus, with density, as shown in Table 5. This result indicates that the elastic region and initial stiffness are strongly influenced by the resin density. The test results obtained for the two types of resin in unconfined expansion are reported in Table 5 in terms of the Young's modulus (E) and failure stress (r_u). Due to the different number of replicates, the standard deviations of both the failure stress and Young's modulus, for each type of specimen, are also reported in Table 5.

It is worth noting that resin HDR-A-10, which had been prepared under the higher confinement pressure (935 kPa) and thus, had a greater density, exhibited a more pronounced kink due to a higher initial modulus (Fig. 10). Conversely, HDR-B-1 and HDR-B-3 showed extremely similar behaviour, except for the stress level at failure (Fig. 11). From Fig. 12, it can be observed that the radial strains at failure may be influenced by the confinement pressure and density of the specimens. Indeed, specimens exhibiting lower values of confinement pressure and density are capable of deforming much more before the damage becomes great enough to initiate unrecoverable damage.

The mechanical properties of all the tested resins were correlated to the density of the single type of specimen. Figs. 13 and 14 show the relationships between the failure stress (r_u) against density and Young's modulus (E) against density, respectively. It can be observed that these properties are strongly correlated to the density of the material and that this dependence is extremely similar to a simple exponential law. The yield radial strain ($e_{r,y}$) and density (q) are also well correlated with each other, as shown in Fig. 15, according to the law, $e_{r,y} = a \cdot q^{b}$ (with $a = 2.468 \cdot 10^{3}$ and b = 1.11), irrespective of the type of resin. These results are consistent with those reported by

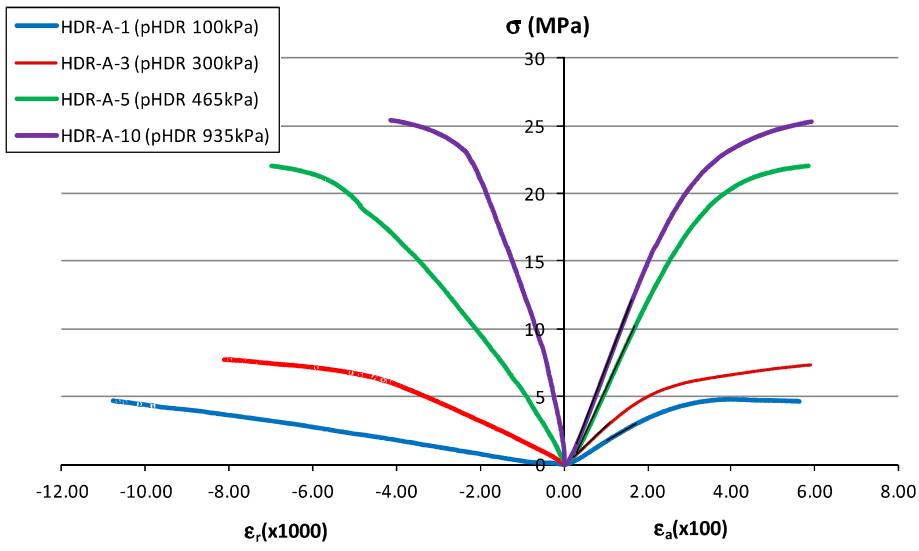

Fig. 10. Mechanical response of HDR-A in Unconfined Compression Strength Tests (UCS): stress–axial strain and stress–radial strain behaviours (pHDR in kPa).

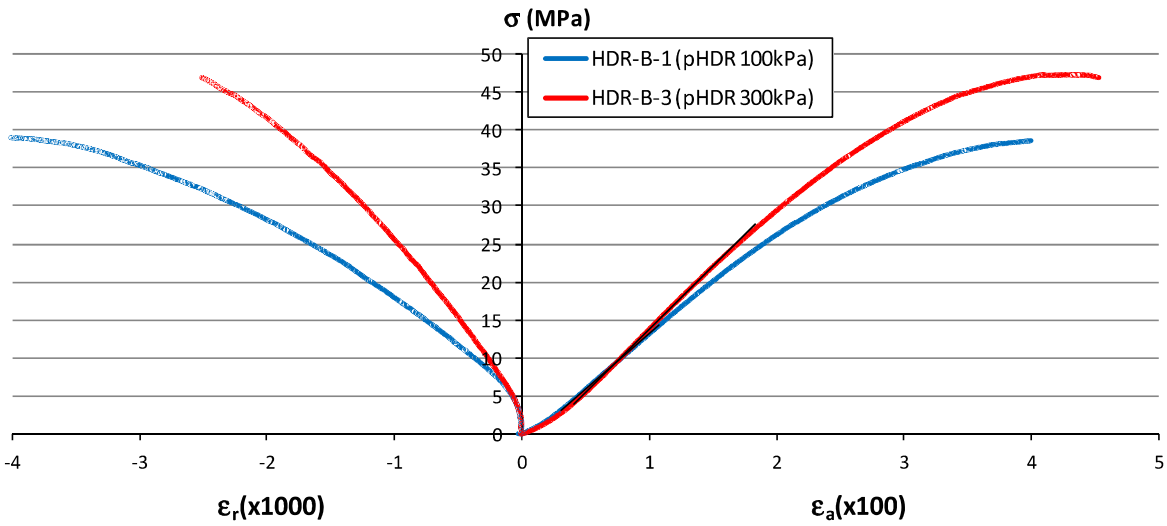

Fig. 11. Mechanical response of HDR-B in Unconfined Compression Strength Tests (UCS): stress–axial strain and stress–radial strain behaviours (pHDR in kPa).

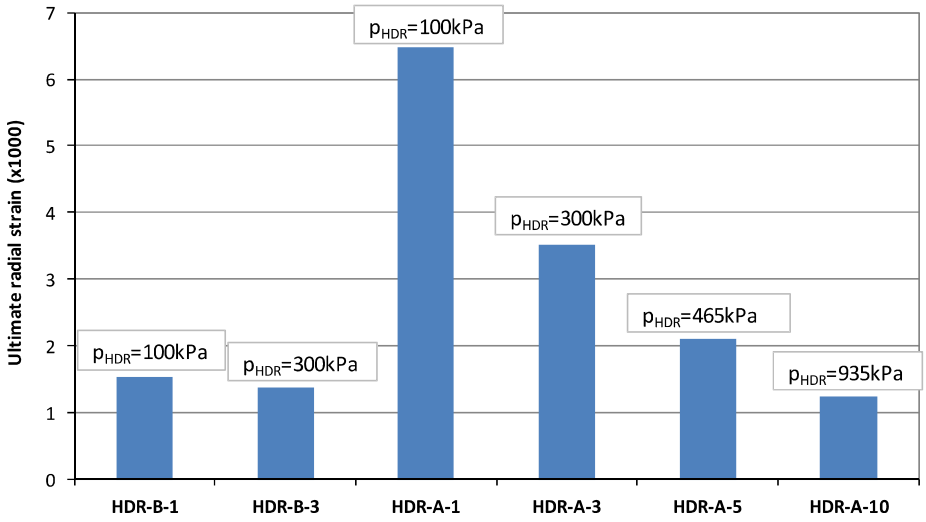

Fig. 12. Ultimate radial strain of the different resin specimens.

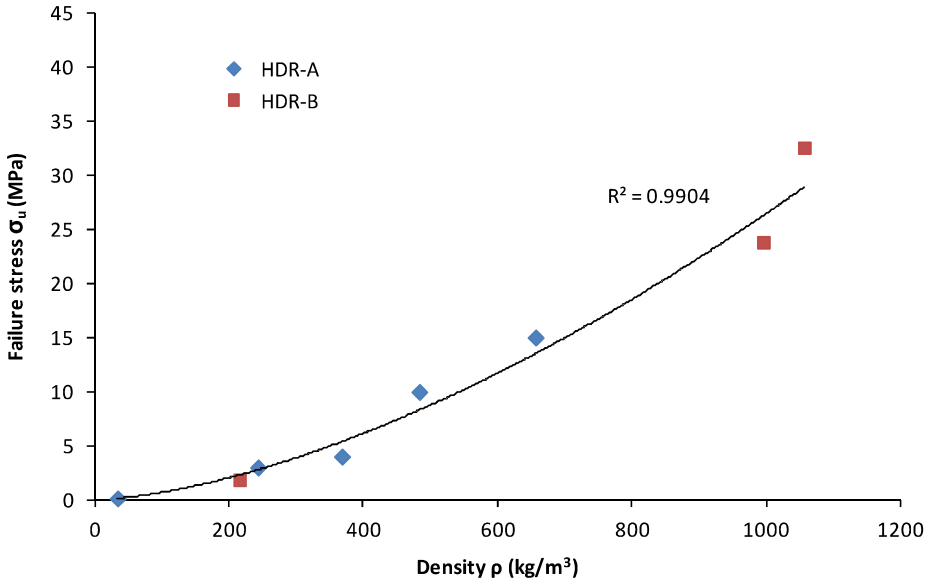

Fig. 13. Relationship between ultimate strength and density of the tested specimens.

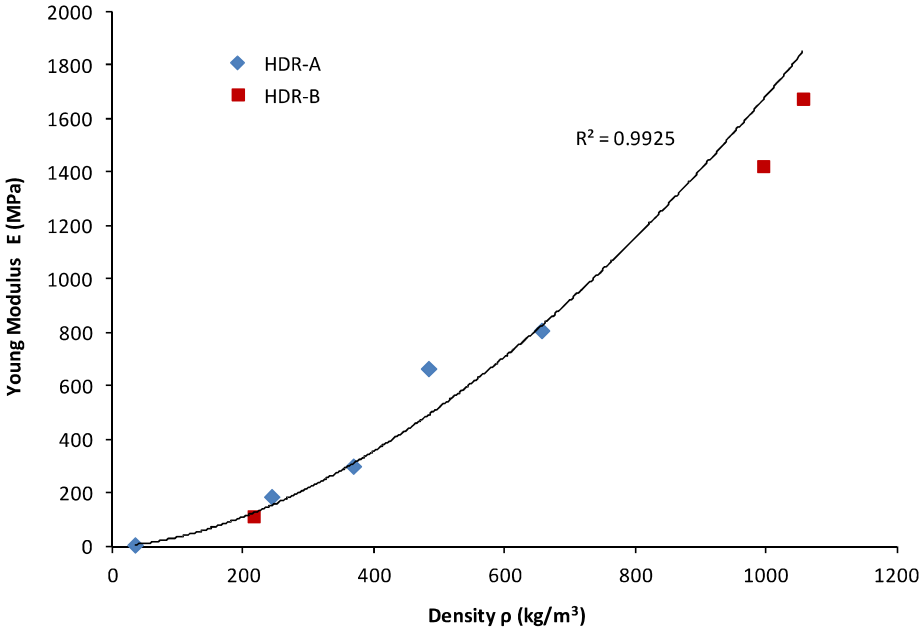

Fig. 14. Relationship between Young modulus and density of the tested specimens.

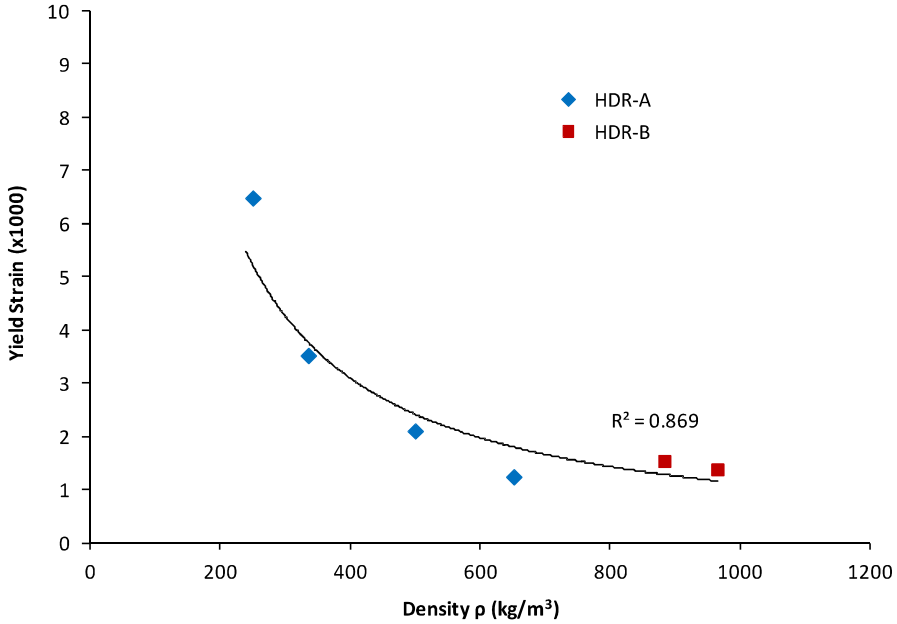

Fig. 15. Relationship between yield strain and density of the tested confined specimens.

Saha et al. (2005), who investigated the effect of the density, microstructure and strain rate on the compression behaviour of polymeric foams. The researchers determined that the peak stress and energy absorption are strongly dependent on the density of the material and that this relationship can be easily described using a power law.

A further fundamental property, called the fracture energy density (FE), was evaluated from the UCS test results. FE is an energy threshold that defines the development of macro-cracks at any time during either crack initiation or propagation at any point in the material. Thus, the fracture energy density corresponds to the energy required to fracture the specimen, and it is easily determined as the area under the stress–strain curve at the failure point (Zhang et al., 2001). A comparison between the fracture energy densities obtained from the resin specimens at different confinement conditions are shown in Fig. 16.

It can be observed that the energy required to incur failure in the resins is material dependent with a minor influence from both confinement and density. In fact, FE values of the HDR-A resins are extremely similar (from 9 kJ/m ^{3} to 11 kJ/m^3). The same trend can be observed among the HDR-B resins, which had FE values ranging from 23 kJ/m ^{3} to 26 kJ/m ^{3}. A larger difference can be observed by com-

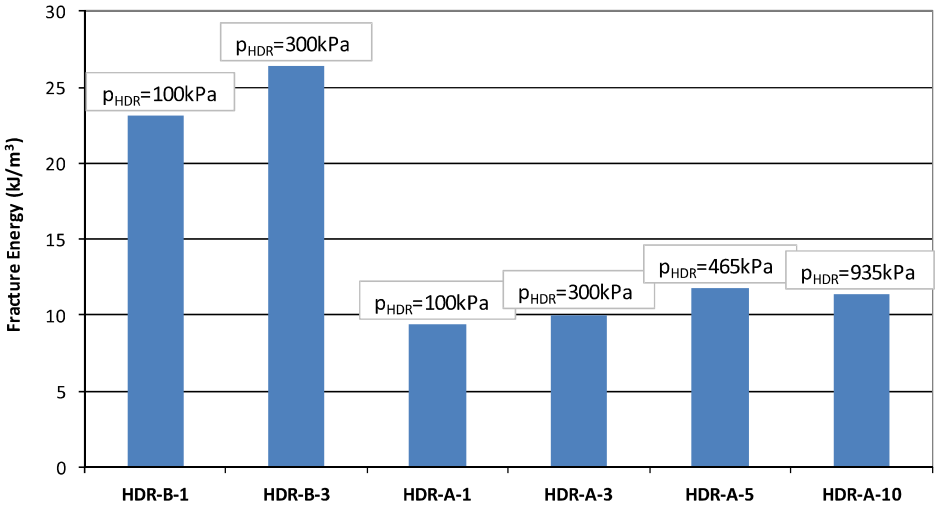

Fig. 16. Fracture energy from resin specimens at different confinement conditions.

paring the fracture energy densities of the two types of resins: HDR-B FE is twice that of the HDR-A FE.

It must be noted that even if the HDR-B resins exhibit significantly higher fracture energies, these resins exhibit extremely low ultimate radial strains compared with that of the HDR-A resins. This result is attributable to the different overall behaviour of the two types of resins: HDR-B exhibits a better resistance to failure but a lower ability to deform, whereas HDR-A has the ability to deform much more before the damage becomes great enough to cause failure.

4. Conclusions

The experimental research described in this paper represents a contribution towards defining a standard design procedure to use polyurethane expanding resins for geotechnical problems.

Two types of resins commonly used for geotechnical applications were analysed: HDR-A, which is characterised by a relatively high expanding power and a lower strength level, and HDR-B, which is characterised by a lower expanding power with respect to HDR-A and a higher strength level at the same confinement pressure.

The first objective of the study was to determine the relationship between the confinement pressure (p_{HDR}) during expansion and the density of the analysed resins at solid state. For this purpose, a laboratory pressure device was set up to prepare the resin specimens under different confinement conditions. The experimental measurements show how the resin density and confinement pressure are linked by a well-defined law, in which, for the same type of resin under confined conditions, the mechanical work is constant.

The microstructural characteristics of different resin specimens were analysed using scanning electron microscope images to understand the mechanical aspects investigated in the second stage of the study.

The second objective of the study was to investigate the mechanical behaviour of the different types of resins under quasi-static unconfined compression tests. A series of 44 resin specimens were tested in the thickness (rise) direction, and the stress–strain responses were established to determine the peak stress, Young's modulus, and fracture energy densities. Both the peak stress and Young's modulus were found to be dependent on the resin density, whereas the fracture energy density seemed to depend only on the type of resin. In particular, an exponential relationship between the peak stress and resin density and between Young's modulus and resin density were found.

However, several specimens showed a certain level of structural anisotropy, and the mean mechanical behaviour of the different types of resin was found to be not affected by their microstructure.

The results obtained from this study will be useful for engineers that design polyurethane resin applications with the goal to improve the substructure performance of shallow foundations, railway or motorway embankments, and airstrips.

In further studies, it is desirable that both laboratory experiments on the material itself and field tests in actual setup conditions may lead to defining an appropriate design methodology for the use of polyurethane resins as a ground improvement technique.

Acknowledgments

The authors thank Novatek s.r.l. for the financial support of the present research and for kindly providing the HDR pressure device. The authors would also like to thank Filippo Costa for the technical support in the execution of the laboratory tests and Elisa Adorni for her help in acquiring the SEM images. The authors are also extremely grateful to the editor and the two anonymous reviewers for their valuable criticisms and suggestions during the review process.

References

ASTM D 1621-04a, Standard test method for compressive properties of rigid cellular plastics, ASTM International.

ASTM D 695–08, Standard test method for compressive properties of rigid plastics, ASTM International.
Baser, S.A., Khakhar, D.V., 1994a. Modeling of the dynamics of R-11 blown polyurethane foam formation. Polym. Eng. Sci. 34 (8), 632–641.
Baser, S.A., Khakhar, D.V., 1994b. Modeling of the dynamics of water and R-11 blown polyurethane foam formation. Polym. Eng. Sci. 34 (8), 642–649.
Buzzi, O., Fityus, S., Sasaki, Y., Sloan, S., 2008. Structure and properties of expanding polyurethane foam in the context of foundation remediation in expansive soil. Mech. Mater. 40, 1012–1021.
Buzzi, O., Fityus, S., Sloan, S., 2010. Use of expanding polyurethane resin to remediate expansive soil foundations. Can. Geotech. J. 47 (6), 623–634.
Daniel, I.M., Cho, J.M., 2011. Characterization of anisotropic polymeric foam under static and dynamic loading. Exp. Mech. 51, 1395–1403.
Ford, C.M., Gibson, L.J., 1998. Uniaxial strength asymmetry in cellular materials: an analytical model. Int. J. Mech. Sci. 40 (6), 521–531.
Gibson, L.J., Ashby, M.F., 1997. Cellular Solids. Cambridge University Press, Cambridge, UK, 1997.
Hilyard, N.C., Cunningham, A., 1994. Low Density Cellular Plastics. Chapman & Hall, London.
Saha, M.C., Mahfuz, H., Chakravarty, U.K., Uddin, M., Kabir, M.E., Jeelani, S., 2005. Effect of density, microstructure, and strain rate on compression behavior of polymeric foams. Mater. Sci. Eng. A 406, 328–336.
Seo, D., Youn, J.R., 2005. Numerical analysis on reaction injection molding of polyurethane foam by using a finite volume method. Polymer 46, 4682–4693.
Tu, Z.H., Shim, V.P.W., Lim, C.T., 2001. Plastic deformation modes in rigid polyurethane foam under static loading. Int. J. Solids Struct. 38, 9267–9279.
Valentino, R., Romeo, E., Misra, A., 2013. Mechanical aspects of micropiles made of reinforced polyurethane resins. Geotech. Geol. Eng. 31, 463–478.
Zhang, J., Kikuchi, N., Li, V., Yee, A., Nusholtz, G., 1998. Constitutive modeling of polymeric foam material subjected to dynamic crash loading. Int. J. Impact Eng. 21 (5), 369–386.
Zhang, Z., Roque, R., Birgisson, B., Sangpetgnam, B., 2001. Identification and verification of a suitable crack growth law. J. Assoc. Asphalt Pavement Technol. 70, 206–241.